Lithuanian Journal of Physics, Vol. **47**, No. 4, pp. 475–483 (2007)

EFFECT OF THICKNESS OF ULTRA-THIN TIN OXIDE FILM BASED GAS SENSORS *

V. Bukauskas [a], A. Olekas [a], D. Senulienė [a], V. Strazdienė [a], A. Šetkus [a], S. Kačiulis [b], and L. Pandolfi [b]

[a] *Semiconductor Physics Institute, A. Goštauto 11, LT-01108 Vilnius, Lithuania*
E-mail: virgis@pfi.lt
[b] *Institute for the Study of Nanostructured Materials (ISMN-CNR), P.O. Box 10, I-00016 Monterotondo Stazione, Roma, Italy*

Received 28 September 2007; revised 15 October 2007; accepted 21 November 2007

Ultra-thin tin oxide films (of 1–40 nm thickness) for gas sensing were grown by dc-magnetron sputtering. Stoichiometric and stable SnO films were characterized by unexpected dependence of the clean air resistance and the resistance response to H_2, NO_2 gases on the average thickness of the film. The response to gas significantly increased in the extremely thin films. The rate of the sensor response to gas was independent of the thickness. The morphology and chemical composition of the films was analysed by scanning probe microscopy (SPM) and X-ray photoelectron spectroscopy (XPS). The mechanism of the thickness effect on the sensor properties is discussed within the context of development of the part per billion-sensitive miniaturized sensors.

Keywords: gas sensors, metal oxide, resistance response, thickness effect, morphology

PACS: 07.07.Df, 68.37.Ps, 82.80.Pv, 68.55.-a

1. Introduction

During the last decade two aspects of the effect of the dimensions were found highly attractive to investigate in the metal oxide based gas sensor technology [1–7]. First, extreme reduction of the device dimensions (it can be called external dimension effect) is supported by general idea of the miniaturization and integration of the gas sensor systems. In addition, the reduction of the external dimensions of the sensor was proved to be a method for an optimization (or increase) of the device sensitivity. The success of the approach based on the external dimension effect was related to several mechanisms that can be described in terms of gas diffusion, percolation theory, and the surface to volume ratio [2–4].

The second aspect of the effect of the dimensions can be defined as a structural size effect (or an effect of the intrinsic dimensions). Until now different technological methods were proposed for predictable control of the grain size in the polycrystalline metal oxide sensors. It was proved that modification of the grain size results in a definite change of the sensor parameters. Based on an extreme reduction of the size of the structural formations inside the sensitive layers a novel type of the nano-structured sensors has been introduced and intensively investigated within the last few years [5–7].

In present paper a change of the structure of tin oxide layer, achieved by reduction of the thickness of the layer, and electrical properties sensitive to gas were studied. The report deals with the sensor technology that can be applied for modification of the gas sensitivity and the dynamic characteristics of the response to gas of the metal oxide sensors based on the ultra-thin layers.

2. Experimental

2.1. Manufacturing of the sensitive films

Tin oxide films were deposited on a Si based substrate by dc-magnetron sputtering method. Pure tin was sputtered from metallic target in the reactive atmosphere (pressure 355 Pa) composed of a mixture $\mathrm{Ar}:\mathrm{O}_2 = 4:1$. The power density of the magnetron supply during the sputtering was about 0.8 $\mathrm{W/cm}^2$ and

* The report presented at the 37th Lithuanian National Physics Conference, 11–13 June 2007, Vilnius, Lithuania.

ISSN 1648-8504

it was kept the same during the deposition of any series of the oxide films in present work. The temperature of the Si wafer was 573 K. Tin oxide films were uniform in thickness within a circle area of about 1.5 cm in diameter. Thickness of the films was evaluated by the SPM experiments and XPS depth profiling. The SPM method was applied to special samples in which a step-like structure was formed by a mask during the oxide deposition. The height of the step was equal to the film thickness and it was measured by the SPM. In the XPS experiments, the thickness of the films was related to the Ar^+-etching time. The film thickness evaluated by the two methods was almost the same and was proportional to the deposition time. It was found that the relationship between the film thickness (measured in nm) and the deposition time (measured in minutes) was nearly linear and it can be approximated by formula $d_{\mathrm{SnO}} = a \cdot t_{\mathrm{sp}} - b \cdot t_{\mathrm{sp}}^2$. The coefficients in formula $a = 1.7 \cdot 10^{-2}$ nm/s and $b = 5 \cdot 10^{-5}$ nm/s^2. The deposition time t_{sp} typically was from 1 up to 30 minutes and was the only controllable parameter of the technology that was fixed for separate series of the tin oxide film based sensors in this study.

The tin oxide films were grown on Si (100) wafers covered with an insulating SiO_2 layer. The electrical contacts were formed on the top of the films by the sputtering of pure Au through a special mask. On the opposite surface of the Si substrate a mini-heater was formed by standard photolithography before the deposition of tin oxide films. Metal Au film was used for the mini-heater. Dimensions of the single sensor chip were $2 \times 2 \times 0.3$ mm^3. For the gas tests the chip was assembled within a standard TO-39 type transistor package.

2.2. Measurements and conditions

Electrical resistance of the tin oxide films was measured in clean synthetic air and the air containing fixed amount of the impurity gas. During these tests the sensors were fastened within the gas chamber with negligible dead-space volume. The voltage drop across the sensitive film was measured and the resistance of the film was calculated.

Kinetics of the response to a steep change in the gas composition was typically measured for up to 16 sensors at once and at the same conditions. The power supply of the mini-heaters of each sensor was separately set to a fixed magnitude long before the measurements. Consequently, a thermal stability was achieved in the system with the sensors before the electrical measurements. The temperature of each sensor in the chamber was verified by resistive thin Au film thermometer that was also shaped on the substrate on the same surfaces as the mini-heater was made. The tests were performed at different working temperatures from about 525 to about 720 K.

Special gas flow control system was used to produce a controllable change of the gas composition in the sensor chamber. A steep change in the atmosphere composition was produced by switching the chamber inlet from the clean air channel to the channel in which the contaminated air flowed. Synthetic air was flowing at the same constant rate (typically about 205 standard cubic centimetres / 200 ml per minute) in both of the channels. The connection was changed by special switching valve with the switching time of about 2 ms. More details of this measurement have been previously described in our papers [8–10].

2.3. Surface analysis

Topography of the film surfaces was analysed by D3100 SPM / Nanoscope IVa from Digital Instruments (Veeco Metrology Group). The surface characteristics were mostly measured by standard atomic force microscopy in so-called TappingMode$^{\mathrm{TM}}$. This technique allows high resolution topographic imaging of sample surfaces and does not produce damages of the surfaces. Scans of the surfaces are performed in ambient atmosphere at the room temperature.

Surface roughness measured by the SPM was characterized by power spectral density (PSD) that represents the amplitude of the surface's roughness as a function of the spatial frequency of the roughness. According to the manual of the D3100, the function of the digitized surface profile (height z) is approximated by formula

$$P_{\mathrm{PSD}}(f) = \frac{2d_0}{N} \left| \sum_{n=1}^{N} \exp\left(\frac{\mathrm{i} \cdot 2\pi}{N} (n-1)(m-1) \right) \cdot z(n) \right|^2 ,$$

$$f = \frac{m-1}{N d_0} . \qquad (1)$$

In (1) the surface profile is digitized over length L that is sampled of N points at intervals of d_0, f is spatial frequency, $m = 1, 2, \ldots, N$. Detailed analysis of the PSD will be reported elsewhere. In present study only the total power is used as a characteristic of the surface roughness. The total power P_{PSD} is an integral of $P_{\mathrm{PSD}}(f)$ over the total frequency interval. The square root of the integral equals the standard roughness R_{q},

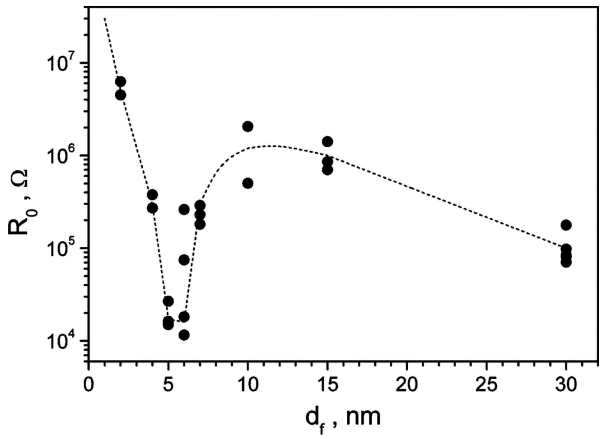

Fig. 1. Clean air resistance measured in separate sensors with fixed tin oxide film thickness (d_f, nm) when the sensor working temperature is $T_w = 525$ K.

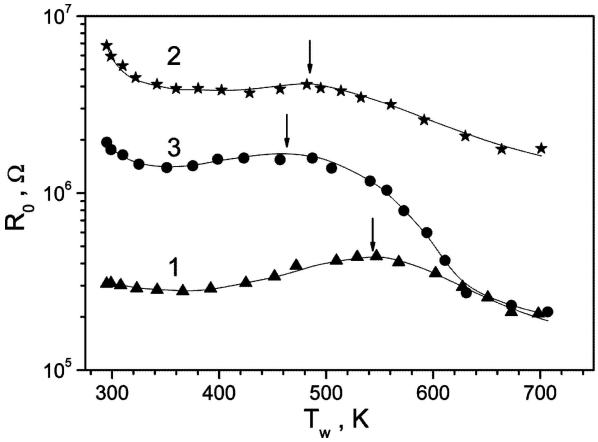

Fig. 2. Dependence of the electrical resistance on temperature for the sensors with fixed thickness of films: 5 nm (*1*), 7 nm (*2*), and 30 nm (*3*). Arrows in figure point to the local maximum of the dependence.

i. e. root mean square (RMS) average of height deviations taken from the mean image data plane.

The selected-area XPS (SA-XPS) measurements and Ar^+ ion sputtering were performed in a VG Escalab MkII spectrometer with 5 channeltron detection system and an unmonochromatized Al K_α source. Dependence of the chemical composition on the film thickness was investigated by combining the XPS analysis and cyclic Ar^+-ion etching (with ion energy $E_i = 2.0$ keV).

3. Results

3.1. Electrical resistance of the films

Reduction in thickness of tin oxide films generally resulted in increase of the resistance of thinner films compared to the thicker ones. Typical correlation between the resistance and film thickness is illustrated in Fig. 1. The results in Fig. 1 were obtained for a series of separated sensors with the oxide films of fixed thickness. The measurements were carried out at the sensor working temperature equal to 525 K.

An unexpected minimum of the resistance was found within the narrow interval of the film thicknesses from about 4 to 7 nm. This minimum was obtained for several series of the sensors separately manufactured over separate periods of the work.

The correlation between the resistance and the thickness shown in Fig. 1 is almost the same at various temperatures from 525 up to about 720 K. Typical dependence of the clean air resistance on temperature is illustrated in Fig. 2. In this figure, the experimental results are presented only for a few sensors with the thickness of tin oxide films corresponding to the most distinct points of the correlation in Fig. 1.

There were no unique variations of the clean air resistance with temperature in ultra-thin tin oxide films compared to relatively thick tin oxide sensors (e. g. [11, 12]). A local maximum in the dependences of the resistance on temperature was typically detected in the ultra-thin tin oxide films at temperatures at which a change between the surface chemisorbed oxygen states O_2^- and the species O^- are known to be the most active. The maximums are pointed by the vertical arrows in Fig. 2. It was determined that the temperature of the resistance maximum decreases with increasing film thickness (550, 480, and 460 K in Fig. 2).

The resistance response to H_2 gas is also unusually dependent on the film thickness in the interval between 4 and 7 nm. Typical results obtained for a series of the sensors based on tin oxide films of fixed thickness are shown in Fig. 3. The resistance response to H_2 gas was measured for the sensors at the working temperature equal to 525 K.

In general, the resistance response of relatively thinner tin oxide films to H_2 gas was higher if $d_f > 7$ nm. For the thinner films, a correlation between the response to gas and the film thickness seems complicated. The sensors based on the oxide film of thickness from 4 to 7 nm are considerably less sensitive than the sensors with relatively thinner and thicker films. The minimum of the response to H_2 gas was observed in the tin oxide films of about 5–6 nm. The thinner films are characterized by relatively higher responses to H_2 gas. Unfortunately, due to technological limitations it was difficult to obtain an accurate relationship between the response and the thickness for the thinnest tin oxide

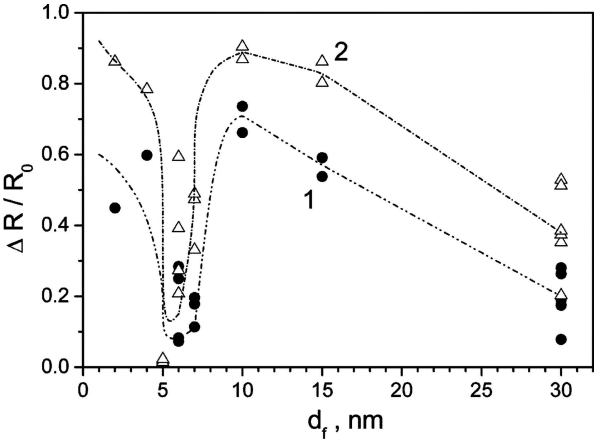

Fig. 3. Relative resistance response to 12 ppm (*1*) and 60 ppm (*2*) of H_2 gas in air measured in separate sensors with fixed tin oxide film thickness d_f when the sensor working temperature is T_w = 525 K. Lines are eye guides.

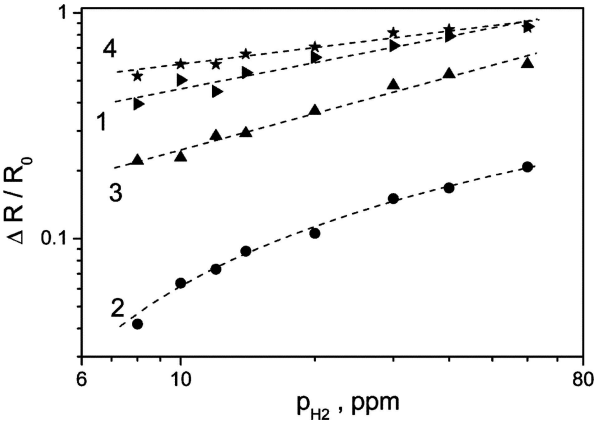

Fig. 4. Dependence of the relative resistance response to H_2 gas in air on the gas partial pressure measured for separate tin oxide films the thickness d_f of which is 2 nm (*1*), 5 nm (*2*), 6 nm (*3*), and 15 nm (*4*). The sensor working temperature T_w = 525 K. Lines are eye guides.

films ($d_f < 5$ nm). It is only clear that the response increases to some extent with decrease of the film thickness when $d_f < 5$ nm.

The relationship between the response to H_2 gas and the thickness shown in Fig. 3 was also obtained in the experiments at various sensor working temperatures from about 525 to 720 K. The correlation in Fig. 3 was also verified by measurements of the response to various concentrations of H_2. Typical results of the response versus H_2 concentration are presented in Fig. 4.

As it can be seen from Fig. 4, there are no vast differences between the sensitivity of the thinner and the thicker tin oxide films. On the other hand, the slope of the dependence in Fig. 4 is higher for thinner films and especially for the film thickness within the interval of 4–7 nm. In general, the dependence of the resistance

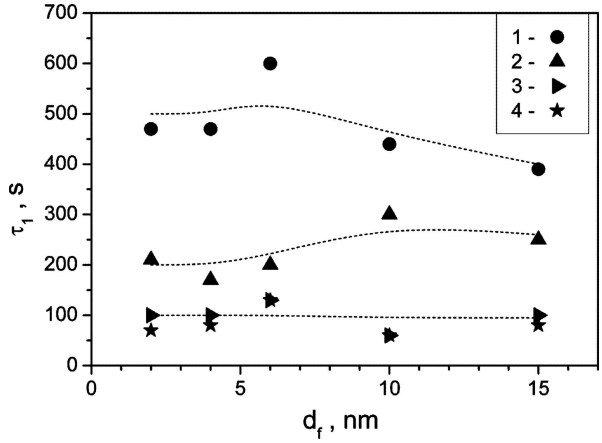

Fig. 5. Time constant of the response of separate SnO_x sensors with fixed film thickness d_f that were exposed to H_2 gas (12 ppm) in air at different working temperatures T_w: *1* at 525, *2* at 575, *3* at 625, *4* at 675 K. Lines are eye guides.

response on gas concentration measured in the ultrathin tin oxide films can be approximated by the same formulas that are commonly used for the description of the resistance response in thick tin oxide devices.

The kinetics of the response was studied and specific parameters were extracted from the experimental results by the method that was thoroughly described in our previous report [13]. According to this method, a transient of the response to a steep change in gas composition was measured. Based on the model in [13] the transients were described by a set of the time constants τ_i that, on the one hand, define the response time of the sensor. On the other hand, these time constants are determined by phenomenological rates of the surface chemical reactions as it has been demonstrated in [13]. It was proved previously [8–10, 13] that the time constant τ_1 is highly dependent on the surface properties of the films and the conditions of the surface chemical reaction.

Typical time constants τ_1 obtained for various sensors based on the oxide film of fixed thickness are plotted as a dependence of the time constant versus film thicknesses in Fig. 5. It has been obtained that the time constant of the sensor response is almost independent of d_f at all the sensor working temperatures from about 525 to 720 K.

It can be recognized that the time constant slightly decreases for the thinnest films. Such change of the time constant is more traceable at lower working temperatures in Fig. 5. In addition, a slight decrease of the time constant was also obtained for the thinnest sensors exposed to NO_2 gas in air. Typical time constants obtained for separate sensors exposed to NO_2 gas are

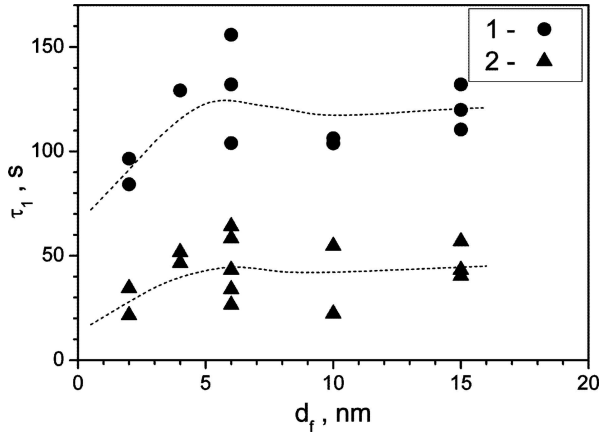

Fig. 6. Time constant of the response of separate SnO_x sensors with fixed film thickness d_f that were exposed to NO_2 gas 10 ppm (*1*) and 20 ppm (*2*) in air at the working temperature of 675 K. Lines are eye guides.

shown in Fig. 6. The working temperature of the sensors was equal to 675 K.

It can be seen from the results in Fig. 6 that the time constant is independent of the tin oxide film thickness if $d_f > 4$ nm. The time constant seems lower for the thinnest films in Fig. 6 ($d_f = 2$ nm). The correlation between the time constant and the film thickness was practically the same at any amount of the target gas (*1* and *2* in Fig. 6). It has been observed in the experiments that the time constant generally decreases for all the sensors if amount of gas is increased (compare *1* and *2* in Fig. 6), as it is typically obtained for the metal oxide gas sensors [13].

3.2. The surface properties

It was found by the atomic force microscopy that topography of the tin oxide film surfaces was dependent on the film thickness. In general, the surfaces seemed smooth with a few distinctive spot-like inclusions in ultra-thin films ($d_f \leq 6$ nm). In medium thin films (6 nm $< d_f \leq 15$ nm), the spot-like inclusions seemed emerging from smooth coverage, evenly spread over the surfaces. Comparatively thick films ($d_f > 15$ nm) were clearly arranged in a granular structure. Typical surface images obtained in the AFM tapping mode are shown in Fig. 7.

The AFM image in Fig. 7(a) was obtained for the films with a thickness of about 2 nm. The surface of these films seems to be homogeneously arranged. Only several columns that are considerably thicker than the total film have been found on these films by AFM analysis. These columns are seen as bright spots in Fig. 7(a). The remaining surfaces of the film look like a flat and slightly rough cover with deeply indented top. The deep indentations seems dividing the layer into flat, smooth, shapeless islands of practically the same height that are tightly packed within the layer and are interconnected. Increase in the film thickness from 2 up to about 15 nm results in considerable increase of

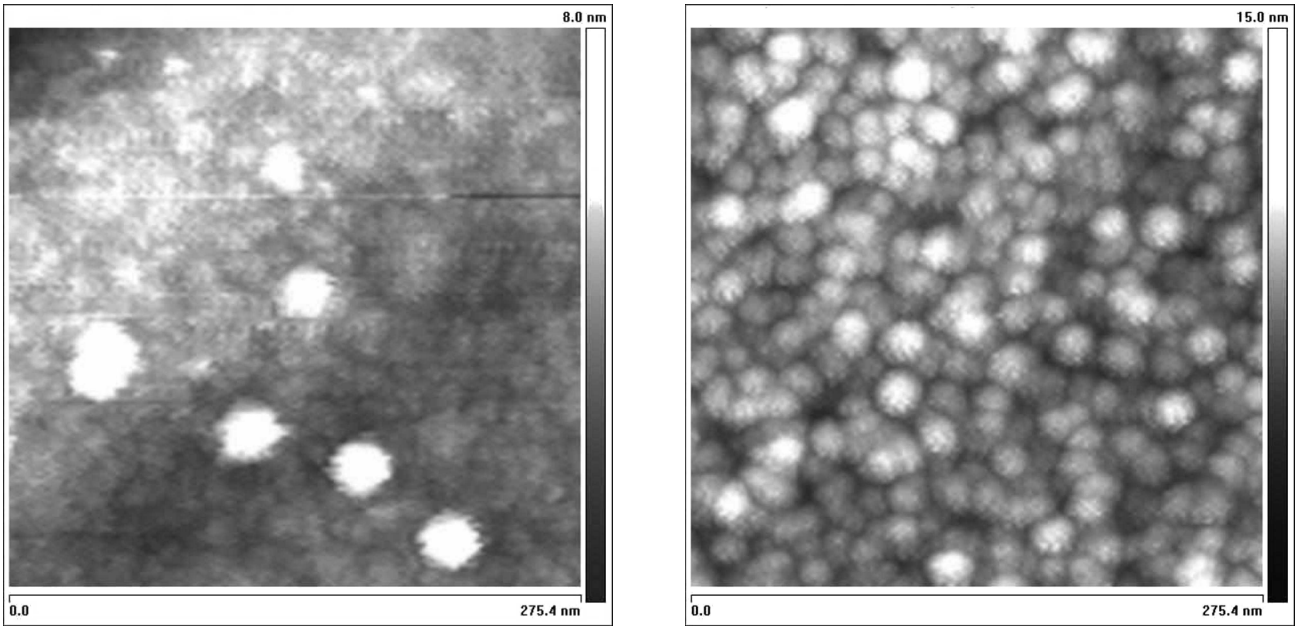

(a) (b)

Fig. 7. AFM image of the surface area 275×275 nm^2 of the tin oxide films of thickness d_f equal to (a) 2 nm and (b) 30 nm. The pale-bright palette of the height scale is 8 nm in (a) and 15 nm in (b).

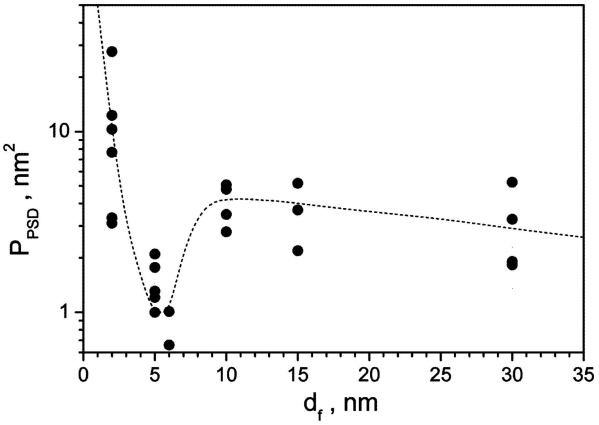

Fig. 8. Integral power $P_{\rm PSD}$ obtained from the analysis of the power spectral density (PSD, Digital Instruments, D3100/ Nanoscope IVa) for the surfaces of the sensors based on ultra-thin SnO_x films of fixed thickness $d_{\rm f}$.

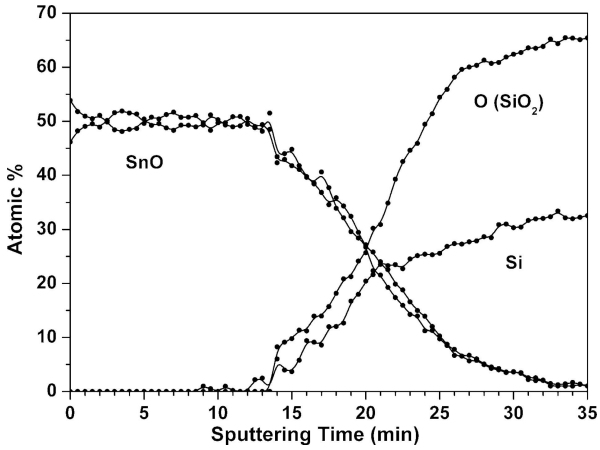

Fig. 9. Depth profile of the gas sensor prepared with 10 minute deposition of SnO_x.

the number of emerging grains that are easy to distinguish within the indented coverage.

The grainy (or possibly pancake shape) structure of the film was clearly seen in the AFM images obtained for comparably thicker films ($d_{\rm f} = 30$ nm). The diameter of the cross-section of the grains in the two-dimensional image is from about 17 to about 23 nm. These objects seem randomly distributed at various depth of the layer and the upper grains partly screen the lower ones. Such distribution suggested that at this stage of film growth there was no column-like arrangement of the grain shape objects in the ultra-thin films of $d_{\rm f} \leq 30$ nm as it was typically found in comparatively thick tin oxide films ($d_{\rm f} > 80$–100 nm, e. g. [14]).

The amplitude of the vertical variation of the ultra-thin film surface line was typically less than the diameter of the grain shape objects (e. g. Fig. 7(a, b)). A dependence of these variations on the film thickness was obtained by the AFM measurements. The roughness of the surfaces of separate sensors based on particular thickness of the film is compared in Fig. 8. In this figure, the roughness of each sensor (a point in Fig. 8) is described by the total power $P_{\rm PSD}$ defined in Section 2.3. The total power $P_{\rm PSD}$ is plotted as a function of the film thickness in Fig. 8.

The parameter of the surface roughness $P_{\rm PSD}$ significantly depends on the film thickness if $d_{\rm f} < 10$ nm. Higher magnitude of $P_{\rm PSD}$ in Fig. 8 can be explained by higher roughness of the surface while lower $P_{\rm PSD}$ characterizes smoother surfaces. As it follows from the results in Fig. 8, the roughest surfaces are obtained for the thinnest films in our study. The minimum in the plot in Fig. 8 suggests that the smoothest surfaces are obtained for the films with a thickness of about 5–6 nm. The films thicker than about 10 nm are characterized by nearly the same $P_{\rm PSD}$ but a slight decrease of $P_{\rm PSD}$ in Fig. 8 can be supposed. This smoothening of the surfaces in the thicker films can be explained assuming more regular distribution of the grain shape objects in thicker films that, consequently, should result in column-like structure of relatively thick polycrystalline tin oxide films.

The surface chemical composition of the samples (averaged through analysed area of about 3 mm in diameter) is characterized by the presence of tin oxide SnO_x with $x \approx 1.3$. In the volume of the films, the chemical composition is constant through the whole thickness with atomic ratio Sn / O ≈ 1 (see Fig. 9). O (SiO_2) and Si lines in the XPS spectrum correspond to SiO_2 layer on Si substrate. This slight reduction of atomic ratio could be caused by the preferential sputtering of oxygen during the depth profiling. However, the shape of valence band spectra (see [12, 15] and references therein) was similar to that of SnO and indicated that the Sn(+2) state remained stable through the whole thickness of the film.

The variation of O $1s$ line after thermal treatment in air is shown in Fig. 10. As a result of this treatment, the component of hydroxyl groups is increased on the sample surface. The third O $1s$ component, which in the fresh sample is attributed to adsorbed water, is also increased after the treatment, but in annealed sample it is totally attributed to SiO_2, i. e. it is the signal from the substrate accompanied by Si $2p$ line. This presence of the substrate signal testifies that the morphology of the sample is changing during the annealing: the film of tin oxide is not anymore uniform. The shape of Sn $3d$ and valence band spectra has not been modified after this treatment. In addition, the value of modified Auger parameter (about 919.2 eV) for main Sn $3d$ and Sn MNN peaks remained constant after the sample annealing and

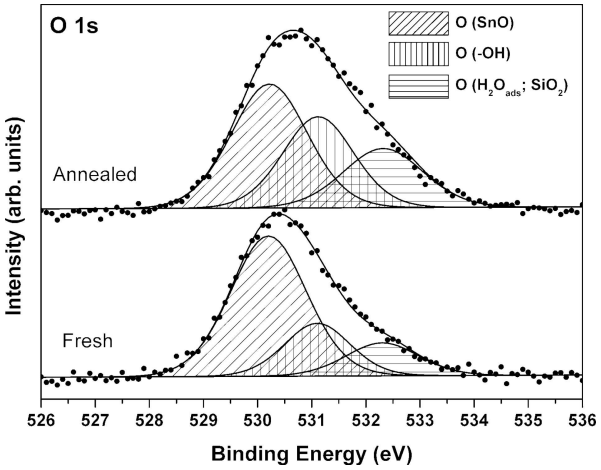

Fig. 10. Typical XPS spectra (O 1s line) of ultra-thin tin oxide film, as-grown (fresh) and after thermal treatment in air at about 700 K for several hours.

confirmed the dominance of Sn(+2) state [15] in all the films investigated.

4. Discussions

It is well known that the properties of thin films vary significantly during the growth and, consequently, are dependent on the film thickness [16–19]. Formation of the films during the physical vapour deposition is determined by the processes that occur in the interface between the solid state and gas [16, 19]. It is commonly accepted [18] that the mechanism of the microstructural evolution of the films is defined by a sequence of the processes, namely nucleation, island growth, impingement and coalescence of the islands, grain coarsening. Termination of the growth "freezes" both the processes at a definite stage and, consequently, the microstructure in the film of a certain thickness. It seems understandable that a dependence of the film properties on the microstructure determines a correlation between the properties and thickness.

In general, nucleation and the island growth should lead to smoothening of the surfaces. This explains a decrease of $P_{\rm PSD}$ in Fig. 9 if comparatively thin films ($d_{\rm f} < 6$ nm) are considered. Growth of the islands results in increase of the necks between the islands and, therefore, the cross-section of the channels for the electric current enlarges in the film. Based on this, it seems understandable that an increase of the film growth time results in decrease of the film resistance as it can be seen in Fig. 1.

Impingement and coalescence of the islands can be influenced by the shadowing effect during the deposition of tin oxide as it is described in [16, 17]. Due to the shadowing, growth of some certain grains (or columns) will be advantageous compared to others. Cavities and hills will be much more distinctive on the surfaces. Consequently, the surfaces of relatively thicker films will be characterized by higher roughness than of the thinner ones. In general, evolution of the film microstructure is related to nonmonotonic changes in the surface roughness that is explained by different film growth models and various mechanisms (see e. g. [18, 19]). Therefore an increase of the integral power $P_{\rm PSD}$ for $d_{\rm f} > 6$ nm in Fig. 9 can be explained by any of the known mechanisms. Unfortunately, at present stage of our investigation the origin of the surface roughening of the films with $d_{\rm f} > 6$ nm is not clear and more detailed investigations are required.

It seems reasonable to suppose that an increase of the surface roughness in the films with 6 nm $< d_{\rm f} <$ 10 nm should lead to reshaping of the electric current channel. A complex net of the connecting necks can be related to an increase of the channel length and decrease in the channel cross-section. Complex pathway for the electron transport can lead to an increase of the clean air resistance as it is in Fig. 1. Nearly constant roughness of the surfaces and slightly decreasing clean air resistance are not understood in present stage of the study.

The resistance response to gas also depends on the tin oxide film thickness (Fig. 3). This dependence qualitatively follows the line of the dependence of the clean air resistance. A decrease in the response of the films with 6 nm $< d_{\rm f} <$ 10 nm can be understood if one supposes that smoothening of the film surfaces results in a decrease of the surface area which can be accessed by gas particles. Roughening of the film surfaces should result in increase of the surfaces exposed to gas and, consequently, these changes can lead to an increase in the resistance response.

It is important to note here that changes in the microstructure and thickness of the film do not produce a related change in the time constant of the response to gas (Figs. 5 and 6). This result can be understood supposing that the response time depends only on the rates of the surface chemical reactions but is independent on the migration of the chemisorbed gases over the surfaces of tin oxide film. Assuming that the gas particles can access all the reaction sites on the surfaces of the ultra-thin film without a delay it is understandable that the response time of the sensor is independent of the film thickness and even of the microstructure of the film.

5. Conclusions

Series of separated sensors based on tin oxide ultrathin films were prepared by reactive magnetron sputtering in present work. The same technology was used to manufacture all the sensors. The series of the sensors are distinguishable only by thickness of the tin oxide films. The thickness was defined by duration of the deposition of tin oxide films. The clean air resistance, the resistance response, and the response time were measured in these sensors under controlled atmosphere conditions including intentional change of the chemical composition of the gas mixture. Extraordinary dependence of the sensor parameters on the film thickness was obtained by interruption of the deposition at separate stages of the film growth. The most unusual changes in the stationary parameters of the sensors, namely the clean air resistance and the resistance response to gas, are obtained for the films the thickness of which varies from 4 to 6 nm. The dynamic characteristics of the sensors are independent of the growth stage and, consequently, of the film thickness.

The changes in the sensor parameters correlate with the changes in the film morphology and, in particular, with the roughness of the film surfaces. Smooth and homogeneous structures are characterized by comparatively low resistance because of comparatively large cross-section of the electron transport path. In these structures the surface to volume ratio is comparatively low and, consequently, the resistance response decreases significantly. When the columnar structure appears in the films, the electron transport path becomes much more crooked than in the films the growth of which is interrupted at the island formation stage. All these morphological changes do not affect the composition and structure of the surface chemisorption sites. Taking into account that the surface sites determine the rates of the surface chemical reaction one can conclude that the dynamic characteristics of the sensors have to be independent on the film thickness in our study.

Differences in the electrical parameters of tin oxide film gas sensors of fixed thickness can not be adequately explained by gas diffusion based model. An increase of the film thickness when the columnar structure of the film is formed must result in increase of the diffusion time. Consequently, the response time of the sensor has to be longer for the sensors with thicker tin oxide film. This assumption is not supported by our results of the response kinetics. Therefore it seems that the results of our study do not support the model of gas diffusion into the depth of the ultra-thin metal oxide films. The results are much more explainable in terms of the percolation theory assuming a dependence of the channel network parameters on the thickness of the films as it has been described in previous paragraph of this section. On the other hand, it has to be noted here that detailed interpretation of the dependences obtained in present study requires additional investigation of the correlation between the electrical parameters and the film morphology in tin oxide based gas sensors.

Acknowledgement

The study in SPI (Vilnius) has been funded by the European project WOUNDMONITOR.

References

[1] A. D'Amico, C. Di Natale, E. Martinelli, L. Sandro, and G. Baccarani, Sensors small and numerous: Always a winnig strategy?, Sens. Actuators B **106**, 144–152 (2005).

[2] J. Klober, M. Ludwig, and H.A. Schneider, Effects of thickness and additives on thin-film SnO_2 gas sensor, Sens. Actuators B **3**, 69–74 (1991).

[3] S. Altieri, L.H. Tjeng, and G.A. Sawatzky, Ultrathin oxide films on metals: New physics and new chemistry?, Thin Solid Films **400**, 9–15 (2001).

[4] N. Matsunaga, G. Sakai, K. Shimanoe, and N. Yamazoe, Diffusion equation-based study of thin film semiconductor gas sensor-response transient, Sens. Actuators B **83**, 216–221 (2002).

[5] G. Blaser, Th. Ruhl, C. Diehl, M. Ulrich, and D. Kohl, Nanostructured semiconductor gas sensors to overcome sensitivity limitations due to percolation effects, Physica A **266**, 218–223 (1999).

[6] N. Yamazoe, Toward innovations of gas sensor technology, Sens. Actuators B **108**, 2–14 (2005).

[7] E. Comini, G. Faglia, G. Sberveglieri, D. Calestani, L. Zanotti, and M. Zha, Tin oxide nanobelts electrical and sensing properties, Sens. Actuators B **111–112**, 2–6 (2005).

[8] A. Galdikas, Ž. Kancleris, D. Senulienė, and A. Šetkus, Influence of heterogeneous reaction rate on response kinetics of metal oxide sensors to gas: Application to the recognition of an odour, Sens. Actuators B **95**, 244–251 (2003).

[9] A. Šetkus, C. Baratto, E. Comini, G. Faglia, A. Galdikas, Ž. Kancleris, G. Sberveglieri, and D. Senulienė, Influence of metallic impurities on response kinetics in metal oxide thin film gas sensors, Sens. Actuators B **103**, 448–456 (2004).

[10] A. Šetkus, S. Kaciulis, L. Pandolfi, D. Senulienė, and V. Strazdienė, Tuning of the response kinetics by the impurity concentration in metal oxide gas sensors, Sens. Actuators B **111–112**, 36–44 (2005).

[11] G. Gaggiotti, A. Galdikas, S. Kačiulis, G. Mattogno, and A. Šetkus, Temperature dependencies of sensitivity and surface chemical composition of SnO_x gas sensors, Sens. Actuators B **24–25**, 516–519 (1995).
[12] G. Gaggiotti, A. Galdikas, S. Kačiulis, G. Mattogno, and A. Šetkus, Surface chemical composition study of tin oxide based gas sensors, J. Appl. Phys. **76**, 4467–4471 (1994).
[13] A. Šetkus, Heterogeneous reaction rate based description of the response kinetics in metal oxide gas sensors, Sens. Actuators B **87**, 346–357 (2002).
[14] A. Galdikas, V. Jasutis, S. Kačiulis, G. Mattogno, A. Mironas, V. Olevano, D. Senulienė, and A. Šetkus, Peculiarities of surface doping with Cu in SnO_2-thin film gas sensors, Sens. Actuators B **43**, 140–146 (1997).
[15] A.R. González-Elipe, V. Jiménez, A. Fernández, and J.P. Espinós, Interface effects for metal oxide thin films deposited on another metal oxide: I. SnO deposited on SiO_2, Surf. Sci. **350**, 123–135 (1996).
[16] R.P.U. Karunasiri, R. Bruinsma, and J. Rudnick, Thin-film growth and shadow instability, Phys. Rev. Lett. **62**, 788–791 (1989).
[17] F. Ying, R.W. Smith, and D.J. Srolovitz, The mechanism of texture formation during film growth: The roles of preferential sputtering and shadowing, Appl. Phys. Lett. **69**, 3007–3009 (1996).
[18] I. Petrov, P.B. Bama, L. Hultman, and J.E. Greene, Microstructural evolution during film growth, J. Vac. Sci. Technol. A **21**, 117–128 (2003).
[19] C. Friesen, S.C. Seel, and C.V. Thompson, Reversible stress changes at all stages of Volmer–Weber film growth, J. Appl. Phys. **95**, 1011–1020 (2004).

LABAI PLONŲ ALAVO OKSIDO SLUOKSNIŲ STORIO ĮTAKA DUJŲ JUTIKLIŲ PARAMETRAMS

V. Bukauskas [a], A. Olekas [a], D. Senulienė [a], V. Strazdienė [a], A. Šetkus [a], S. Kačiulis [b], L. Pandolfi [b]

[a] *Puslaidininkių fizikos institutas, Vilnius, Lietuva*
[b] *Nanosandaros medžiagų tyrimo institutas, Monterotondo Stacione, Roma, Italija*

Santrauka

Magnetroninio dulkinimo būdu užaugintų plonų (1–40 nm storio) H_2 ir NO_2 dujoms jautrių alavo oksido sluoksnių pagrindu pagamintos kelios serijos skirtingų jutiklių. Jutikliai skyrėsi vien tik alavo oksido sluoksnio storiu. Jutiklių parametrai (elektrinė varža švariame ore, varžos atsakas į dujas ir atsako laikas) buvo matuojami juos patalpinus kameroje su valdoma atmosfera. Savo stacionariais parametrais labiausiai išsiskyrė jutikliai su 4–6 nm storio SnO_x sluoksniais, o dinaminiai parametrai nepriklausė nuo dujoms jautraus sluoksnio storio. Jutiklio parametrų pokyčiai atitiko SnO_x sluoksnių morfologijos kitimą (ypatingai lygumą). Sluoksnių morfologijai ir cheminei sudėčiai tirti panaudoti skenuojančio zondo mikroskopas (SZM) ir Rentgeno fotoelektronų spektroskopas. Tyrimų rezultatai rodo, kad ploniems ($<$100 nm) metalų oksidų sluoksniams dujų difuzijos į gylį modelis netinka. Rezultatai paaiškinami elektrinės srovės kanalų tinklo kitimu esant skirtingam sluoksnių storiui.